MOLECULAR PHYSICS e2341111
https://doi.org/10.1080/00268976.2024.2341111

Taylor & Francis
Taylor & Francis Group

RESEARCH ARTICLE

Interfacial structure within thin films of decane isomers adsorbed on a metal substrate

Michael W. Haslam and Kelly E. Anderson

Department of Chemistry, Roanoke College, Salem, VA, USA

ABSTRACT

Canonical-ensemble Monte Carlo simulations were used to examine the solid–liquid interfacial structure within neat and multicomponent solutions of decane isomers at 350 K. As seen both experimentally and computationally for many fluids, layering within the liquid film near the solid substrate was exhibited in all fluids examined here. The amount of branching within a molecule, though, limited the range of density oscillations, particularly for multicomponent fluids. Analysis of molecular orientation within the first layer showed a strong preference in most cases for molecules to adopt orientations that enhance the energy of adsorption. To this end, preferential absorption was observed in all fluid mixtures with *n*-decane present. For both *n*-decane and 2,2-dimethyloctane, whether neat or in solution, the preference for orientations that maximise interactions between the alkane backbone of the molecule and the substrate led to additional in-plane alignment between adjacent adsorbed molecules. In contrast, for 4-propylheptane little in-plane alignment or orientation preference was observed at the interface.

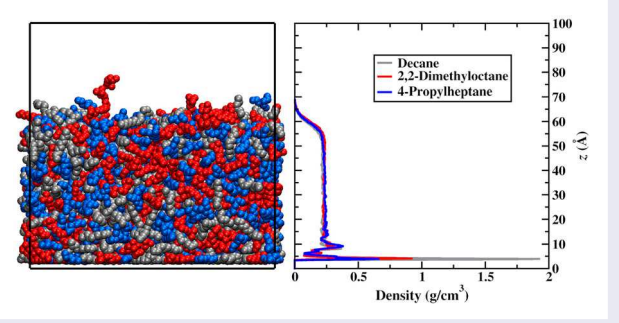

ARTICLE HISTORY
Received 8 January 2024
Accepted 2 April 2024

KEYWORDS
Surface adsorption; Monte Carlo simulations; branched alkanes

1. Introduction

In the past 70 years, a number of important analytical developments expanded our ability to probe interactions at the liquid–solid interface [1–3]. Interfacial effects, including increased viscosity and induced structural order, have been observed both experimentally and via simulation [4–9]. As a result of the varied applications of solid–liquid interfacial effects, these systems have been studied extensively using molecular simulation and density functional theory. While many studies focus on one-component fluid phases, multi-component liquid films and droplets are of interest for applications such as lubricants, separations, catalysis, and in environmental systems. Model systems, such as Lennard-Jones particles or hard cylinders, provide an avenue to probe the fundamental properties of adsorption from mixtures. Examples include variations in unlike intermolecular interactions between fluid components in symmetric mixtures [10–13], adsorption from asymmetric binary mixtures [14–17], the influence of solid–fluid interaction strength [12,13,18–20], and the role of molecular shape or size [21–26].

Studies of molecular systems build on these model studies to gain insight into molecular-level adsorption behaviour. Competitive adsorption is observed from liquid mixtures of alkanes [7,27–38], halohydrocarbons [39–42], water–alcohol solutions [42–50], water–acetonitrile [51–54], acetone–chloroform [55],

CONTACT Kelly E. Anderson kanderson@roanoke.edu Department of Chemistry, Roanoke College, Salem, VA 24153, USA

Supplemental data for this article can be accessed online at http://dx.doi.org/10.1080/00268976.2024.2341111.

and salt water–acid solutions [56]. These studies feature many types of surfaces, different intermolecular interactions, varying molecular sizes and shapes, and different surface architectures. Preferential adsorption results in variations in composition as a function of position within the film or droplet. The impact of this variation is of great importance for understanding processes directly at the solid–liquid interface, such as wetting [42–44,47,49].

Simulation studies allow researchers to examine the structural impacts of adsorption in detail. Experimental studies show that for a variety of types of molecules, including different molecular architectures, oscillations in fluid density occur and vary as a function of surface separation [2,3,5,6,9,57–59]. These density oscillations correspond to the formation of layers within the fluid, an effect that is particularly strong for linear alkanes [5]. Early studies did not show the same effect within liquids composed of branched alkanes, but both experimental and computational studies later confirmed that molecular layering occurs within these liquids as well [7,30,31,60–62].

A number of studies focus on thin films of branched molecules adsorbed onto solid substrates. Examining branched alkane adsorption provides a means to focus on the role of molecular architecture on interfacial properties. Balasubramanian *et al.* [7,29] used Monte Carlo (MC) and molecular dynamics simulations to examine the structural features of thin films of *n*-hexadecane, three branched hexadecane isomers, and squalane adsorbed on a featureless Au(111) substrate. These simulations showed the emergence of density oscillations for all five liquids within 15 Å of the solid substrate. The most highly branched isomer, 2,2,4,4,6,8,8-heptamethylnonane, showed the most interdigitation between the first and second molecular layers and a lower density within the first molecular layer as compared to *n*-hexadecane and the less extensively branched 6-pentylundecane isomer. The lower density of heptamethylnonane within the first layer suggests a less ordered phase adjacent to the substrate.

Wang and Fichthorn [30] examined the effect of chain branching within molecular films of three decane isomers chosen to show the impact of increasing degrees of branching. All three isomers – *n*-decane, 2-methylnonane, and 2,2-dimethyloctane – show layering as a function of distance from the Pt(111) surface. Wang and Fichthorn also looked closely at the ordering of the molecules within the plane adjacent to the Pt surface. All three isomers exhibited in-plane ordering where the long molecular axes align parallel to the substrate and parallel to adjacent adsorbed molecules. In addition, 2,2-dimethyloctane, which had the bulkiest structure, exhibited a 'pillared-layered structure' where a few molecules were aligned with the long molecular axis perpendicular to the interface, forming a molecular pillar between the first and second layers. In these cases, the *t*-butyl end of the molecule was adsorbed at the interface. The presence of these pillared molecules led to an intermediate layer in the centre-of-mass density profile as compared to *n*-decane. The authors concluded that the formation of these pillars is driven by several factors including the bulkiness of the *t*-butyl group reducing the in-plane ordering of adsorbed molecules. This results in a lower density of molecules within the first layer and, thus, spaces between the molecules adsorbed parallel to the substrate. These spaces allow for the *t*-butyl groups of nearby molecules to adsorb at the interface.

Wang and Fichthorn [31] followed this work by looking at the effects of confinement on the structure of branched alkane fluids. As in the free-standing film, they note the formation of layers within the fluid adjacent to both solid–liquid interfaces as well as the adsorption of a few molecules that bridge adjacent layers, i.e. a pillared-layered structure. In contrast to the stepwise changes in density between the surfaces that are observed for linear molecules as whole layers are added or squeezed out, as the distance between the surfaces changes, a smoother transition is observed for branched alkanes. In these fluids, the molecules transition between parallel and perpendicular alignments with respect to the surfaces such that the changes in density are less abrupt.

The majority of the existing simulations exploring the structural features of branched alkane films adjacent to solid substrates have focussed on one-component fluids. In this work, we expand on these studies to examine the impact of branching on adsorption from multicomponent fluid phases. In our previous work [34], we found that preferential adsorption from mixtures of linear alkanes was observed even when the alkanes differed by only one methylene unit. Here, we look at isomers of decane and explore how branching impacts adsorption.

2. Simulation details

Monte Carlo simulations for all fluid phases were completed in the canonical (*NVT*) ensemble using Monte Carlo for Complex Chemical Systems-Minnesota [63]. Three isomers of decane were examined here: *n*-decane (DEC), 2,2-dimethyloctane (OCT), and 4-propylheptane (HEPT). Each simulated fluid consisted of a thin, liquid film composed of 1700 molecules (1701 for the ternary solution) with the substrate surface located at $z = 0$ and a vapour–liquid interface at the other edge of the film. A rectangular simulation cell with dimensions 100 Å × 100 Å in the *xy* place was used. A ceiling was applied at 100 Å from the substrate interface, which was

at least 30 Å above the liquid surface, similar to other recent studies [35,50]. This ceiling was applied to keep molecules from leaving the system. Periodic boundaries were applied in the x and y directions only.

Seven fluids composed of the three decane isomers were examined: neat liquids of each isomer; equimolar binary mixtures of DEC–OCT, DEC–HEPT, and OCT–HEPT; and an equimolar solution of all three isomers. Each film was simulated at 350 K. Four independent simulations were completed for each, starting from different initial distributions for the binary and ternary mixtures. At least 250,000 MC cycles (where 1 cycle $= N$ MC moves) were completed to equilibrate each simulation, and results were tabulated for an additional 250,000 MC cycles. The statistical uncertainties reflect the standard error of the mean determined from the four independent simulations. For all simulations, the standard MC moves were used: centre-of-mass translations and rotations, and configurational-bias Monte Carlo (CBMC) conformation sampling [64–66]. For one-component fluids, moves were chosen as follows: 30% CBMC, 35% translation, and 35% rotation. For the binary and ternary mixtures, CBMC identity exchange moves were also employed to facilitate better sampling [67,68]. The resulting distribution of moves types was 20% identity exchange, 20% CMBC, 30% each, translations and rotations. During all CBMC regrowth steps involving conformational moves and identity switch moves, 10 trial positions were explored. This choice has been shown previously to provide satisfactory sampling efficiency for united-atom alkane models [69,70].

Many force fields are available throughout the literature to model linear and branched alkanes [71,72]. Recent work comparing all-atom, united-atom, and coarse-grained force fields showed that the choice of potential form is particularly important for examining thermophysical properties, such as density, viscosity and self-diffusion, under extreme conditions [73]. Here, the transferable potentials for phase equilibria–united atom (TraPPE) force field was chosen in light of its previous use to examine adsorption properties, the mild simulation conditions, and good agreement with experiment for liquid phase structural properties [34,60,66,69,74].

Within the TraPPE force field, the 12–6 Lennard-Jones potential is used to describe nonbonded interactions, a cosine series for dihedral (1–4) interactions, and a harmonic potential for angle bending [66,75]. All bond lengths were kept fixed. Unlike interactions were modelled using the Lorentz-Berthelot combining rules. A 14 Å cutoff was used for all alkane–alkane interactions. No cutoff was used for surface–alkane interactions.

The choice of solid–fluid interaction force field is very important for adsorption studies as the resulting behaviour will be strongly influenced by this choice [49,76–81]. Here, alkane–substrate interactions were described using the Hautmann–Klein 12–3 potential with parameters appropriate for a smooth Au(111) substrate [82]. Additional parameters for CH and C interactions with the substrate were taken from the work of Potoff and Siepmann [60]. The parameterisation of this model was developed to examine the structure of alkyl thiols chemisorbed onto Au(111). This work found that using a 12–3 potential form to describe the interactions of the physisorbed alkane interaction sites with the surface better reproduced the binding energy, distance from the surface, and dispersion coefficient than a 9–3 potential form [82]. Balasubramanian et al. [7,29] showed that the Hautman–Klein 12–3 potential is able to describe the heats of adsorption for linear alkanes in very good agreement with experimental findings for both single atom adsorption and multilayer films. Additionally, this interaction potential is able to reproduce the density oscillations observed near solid surfaces for both linear and branched alkane films, 2D critical properties for adsorbed alkane monolayers, and the experimental preferential adsorption behaviour in mixtures of similarly-sized linear alkanes [7,29,34,60,83–85].

3. Results and discussion

Images of the side view of the films and top view of the first adsorbed layer are shown for each system in Figures 1 and 2.

3.1. Density profiles

Centre-of-mass (COM) density profiles for each isomer – n-decane (DEC), 2,2-dimethyloctane (OCT), and 4-propylheptane (HEPT) – are shown in Figure 3. The details of the density profile highlight the structural differences of the molecules. DEC features a clear region of high density at the substrate–liquid interface, near $z = 3.9$ Å, followed by a second region of high density at approximately 8.3 Å and a third near 12.5 Å. The interpeak distance (4.4 Å) is commensurate with the size of a CH_x united atom bead in the TraPPE force field, where $\sigma = 3.95$ Å for CH_2 and $\sigma = 3.75$ Å for CH_3. This behaviour, as is seen for many linear alkanes, arises from molecules adsorbing parallel to the solid interface and molecular layering in the surrounding liquid [5,27,29,34,38,39,58,59,86,87]. The locations of the first three peaks agree well with previous simulations [34,38].

Both branched isomer COM density profiles show similar density oscillations, but the details of these regions vary. For OCT, the location of the first high density region is shifted slightly further from the surface

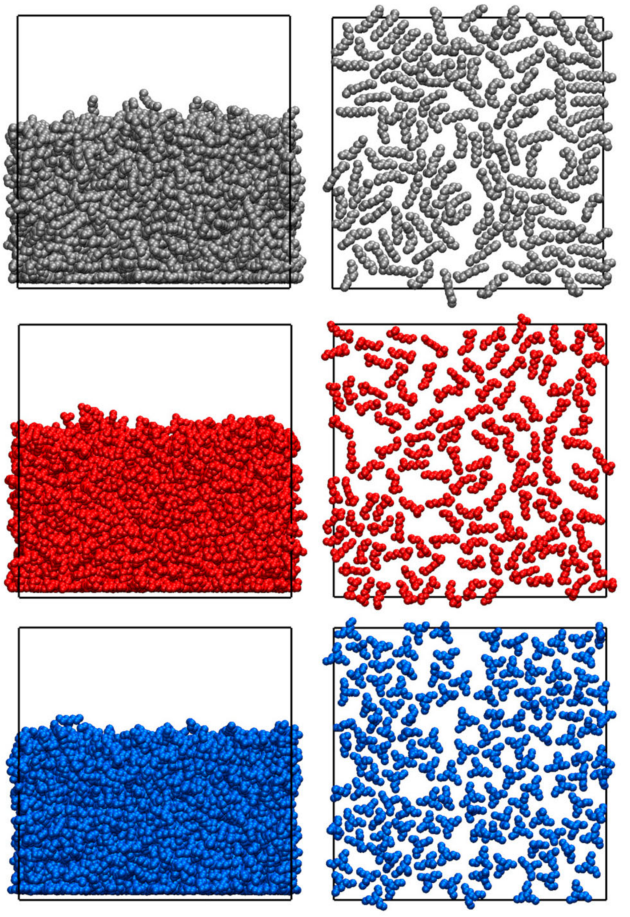

Figure 1. Side view (left) of each neat liquid film and top view (right) of the first adsorbed layer. *n*-Decane is shown at top (grey), 2,2-dimethyloctane in the middle (red), and 4-propylheptane (blue) at bottom.

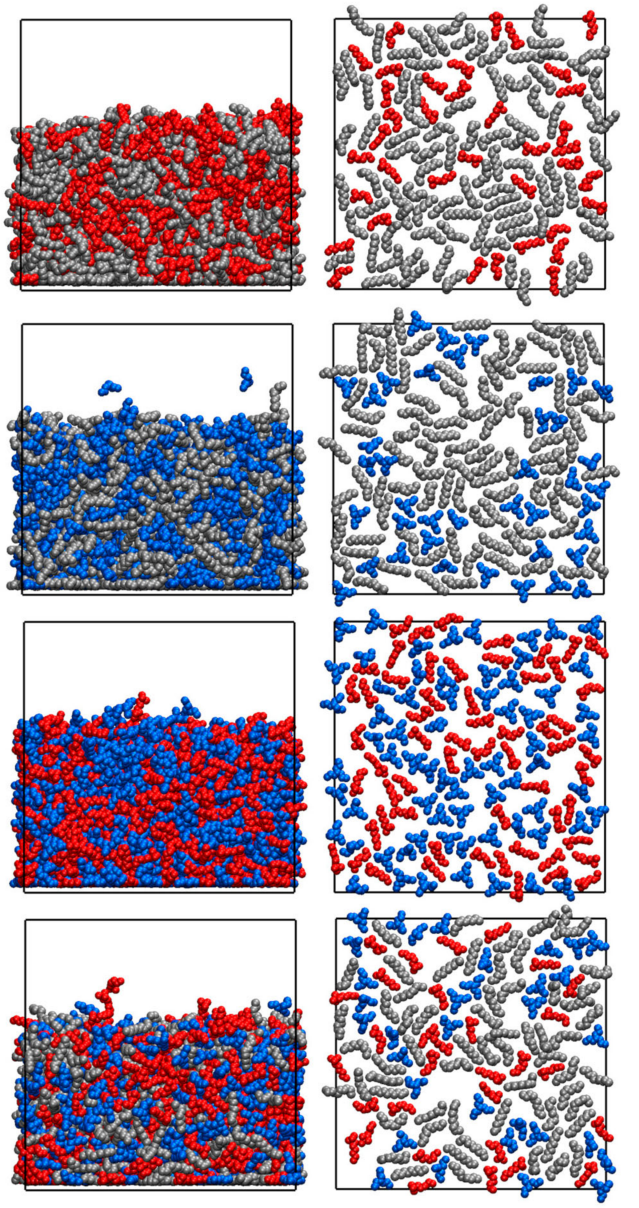

Figure 2. Side view (left) of each liquid film and top view (right) of the first adsorbed layer for binary and ternary liquids. *n*-Decane is shown in grey, 2,2-dimethyloctane in red, and 4-propylheptane in blue. From top to bottom, the solutions are as follows: DEC–OCT, DEC–HEPT, OCT–HEPT, and DEC–OCT–HEPT.

as compared to DEC (Figure 3). The first density peak occurs at 4.1 Å. This is followed by a second, lower density peak at 6.3 Å. A third region where the COM density is slightly higher than the bulk density follows from approximately 8 Å to 12.5 Å, with the peak of this region at approximately 9 Å. For HEPT, the initial high density peak occurs at approximately 3.9 Å, as is observed for DEC. For this molecule, though, the initial peak reaches a lower maximum density than DEC and is marked by a shoulder at 4.7 Å. A somewhat more complicated density oscillation pattern follows the initial peak. It is clear that the different molecular topologies have a strong influence on the density profiles near the solid interface. In all cases, though, by approximately 20 Å, the surface-induced structural features have disappeared and the unstructured liquid is present.

In order to better investigate the density features near the surface, we examined the density profiles for the individual united-atom beads within each molecule (Figure 4). In all three neat liquids, the first peak for each CH_3 profile occurs at 3.5 Å. Similarly, the first peak in the CH_2 profile also occurs at 3.5 Å for all three neat liquids.

The shapes of the two united-atom bead density profiles are very similar to the COM profile for DEC (Figure 3). When we integrate the area under the first peak out to 6.6 Å, we find that the area under the first peak in the CH_2 profile is 3.74 times larger than the area under the first peak in the CH_3 profile, in good agreement with the composition ratio of the molecule $CH_2/CH_3 = 4/1$. Integration values and relative ratios for all fluids are

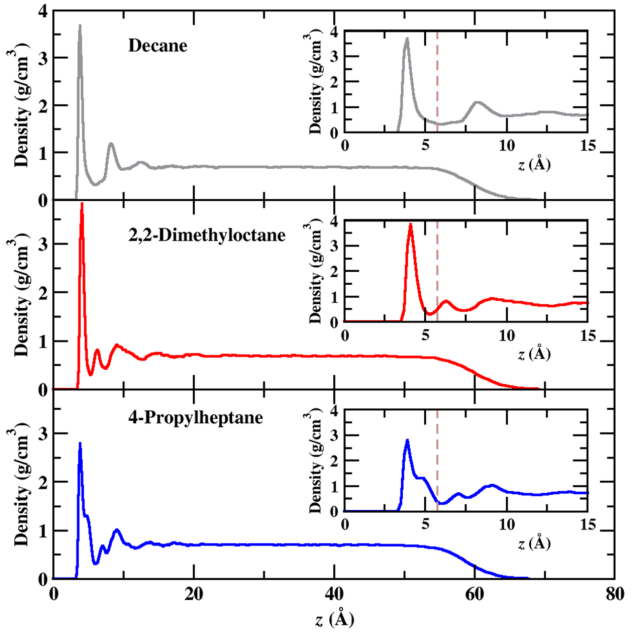

Figure 3. Centre-of-mass density profiles for neat DEC (top, grey), OCT (middle, red), and HEPT (bottom, blue). Each inset figure shows the profile within 20 Å of the interface. The brown dashed line at 5.75 Å is the cutoff used for orientational and surface adsorption analyses.

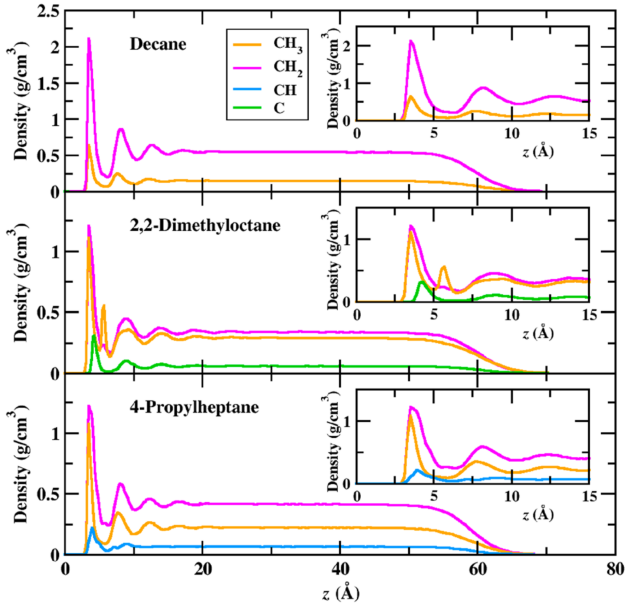

Figure 4. United-atom bead density profiles for DEC (top), OCT (middle), and HEPT (bottom). CH_3 beads are depicted in orange, CH_2 beads in pink, CH beads in green, and C beads in blue. Insets show the profile within 20 Å of the interface.

available in supporting information (Table S1). The integration ratio is consistent with the observation that most of the DEC molecules near the interface are adsorbed with the long molecular axis parallel to the surface so as to maximise the intermolecular interactions.

While the CH_2 profile closely matches the COM profile for DEC, for OCT this is not the case. The first difference is a small secondary peak in the CH_3 profile at 6 Å that is nearly absent in the CH_2 profile. Interactions with the substrate are maximised when the molecule lies with its long axis parallel to the interface. As a result, only two CH_3 groups in the *t*-butyl head group lie directly adjacent to the interface. The remaining CH_3 group lies near, but not directly next to, the substrate leading to the secondary peak evident in the CH_3 profile and the quaternary C group is found slightly further from the surface compared to the CH_2 and CH_3 beads. From the integration of the first peak in these three profiles the ratio of beads present is 5.76/5.01/1.00 (CH_2/CH_3/C). These integrations are taken out to 6.6 Å from the interface. As for DEC, these ratios are very similar to the molecular ratio for OCT (5/4/1, CH_2:CH_3:C), providing evidence for near planar orientations at the interface.

Beyond 6.6 Å, there are additional regions of enhanced density within 25 Å of the interface, including peaks in both the CH_2 and CH_3 profiles near 8.5 Å, 14 Å, and 19 Å. These regions do not include features that distinguish the CH_3 and CH_2 profiles, as is seen closer to the interface. The relative structures of these features seem to be more similar to those observed in DEC, even if they appear at somewhat different distances from the interface.

As noted above, the HEPT COM density profile shows a clear shoulder at 5 Å followed by a very different density oscillation pattern compared to DEC as a result of the propyl side group. From the bead density profile, it is evident that the shoulder is the result of the propyl group as the largest type of united atom group contributing to this peak is CH_2 beads. The COM profile features more oscillations between 5 Å and 10 Å than are seen in the bead profile. This suggests that there are a variety of orientations that the molecule can adopt in the first and second layers adsorption, leading to a broader range of COM positions represented as compared to DEC. From the COM profile, it is clear that the HEPT molecules do not uniformly align themselves at the interface in a particular orientation, as is suggested by the DEC and OCT profiles. Regardless, the peak integration ratio 6.37/3.30/1.00 (CH_2/CH_3/CH) agrees well with the molecular ratio 6/3/1.

Selected COM density profiles of binary mixtures of these isomers are shown in Figures 5–7. The overall density profile and individual profile for each molecule type for the DEC–HEPT mixture is shown in Figure 5. The overall density profile for the mixture is nearly identical to the neat DEC profile (Figure 3), with small differences in the region between 4.5 Å and 8 Å. When the COM density profiles of the molecular species within the mixture are examined, one sees a preference for the

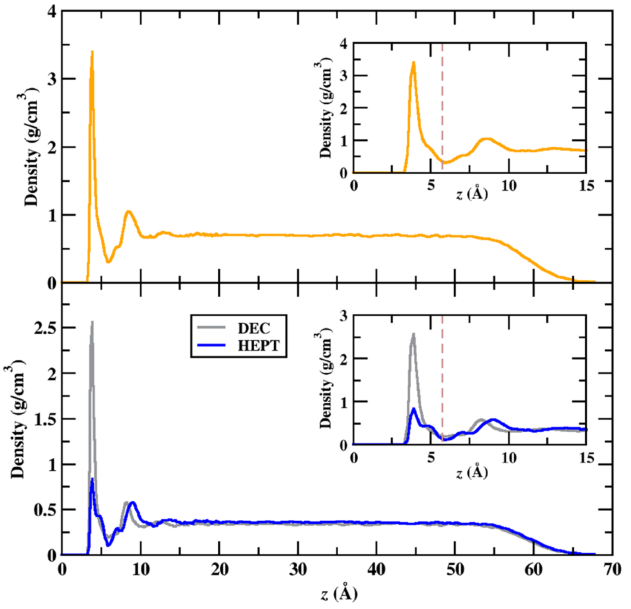

Figure 5. Centre-of-mass density profile for an equimolar mixture of DEC and HEPT. The total density profile is shown at top (orange). In the bottom panel, the density profile for each molecule is shown. DEC is shown in grey and HEPT is shown in blue. Insets show the profile within 20 Å of the interface. The brown dashed line is at 5.75 Å, the cutoff used for orientational and surface adsorption analyses.

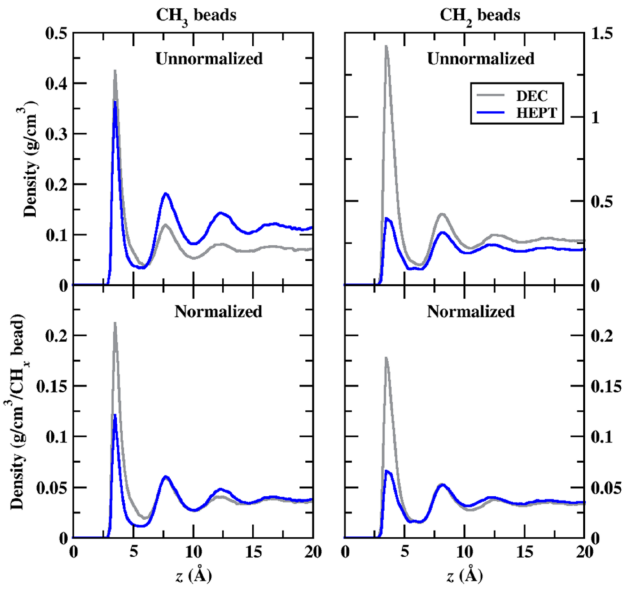

Figure 6. United-atom bead density profiles for an equimolar solution of DEC and HEPT for $z \leq 20$ Å. The left side shows the profiles for CH_3 beads while the profiles for CH_2 beads are shown at right. In the bottom figures, the data are normalised relative to the number of beads of the given type per molecule type. DEC is shown in grey. HEPT is shown in blue.

adsorption of DEC at the surface. It is also clear that the small shoulder in the overall density profile at 4.8 Å is a result of the presence of HEPT adsorbed at the interface, as is true for the feature at 7.2 Å. By 15 Å from the interface, the two species are well-mixed all the way to the vapour–liquid interface.

An examination of the bead density profile for CH_3 groups provides some initial insight into the relative orientations of DEC and HEPT at the interface (Figure 6). The overall density of CH_3 beads from DEC is greater than that of CH_3 beads from HEPT molecules within 6 Å of the interface. When the profiles are normalised for the number of CH_3 beads per molecule, the density of DEC CH_3 beads is nearly twice that of HEPT CH_3 beads. Additionally, this peak does not show the shoulder at 4.8 Å evident in the COM density profile for this solution and for neat HEPT. The lack of an intermediate peak between the initial regions of increased density in the HEPT profile suggests that the propyl arm of the molecule spans from one 'layer' to the next or lies in the plane parallel to the interface.

The overall density profile for the mixture of DEC and OCT strongly reflects the density profile of DEC at distances near the substrate ($z < 10$ Å) with a very small secondary CH_3 peak from OCT and a tail on the second density peak (near 8 Å) reflecting the shift of the second density region away from the substrate as seen in

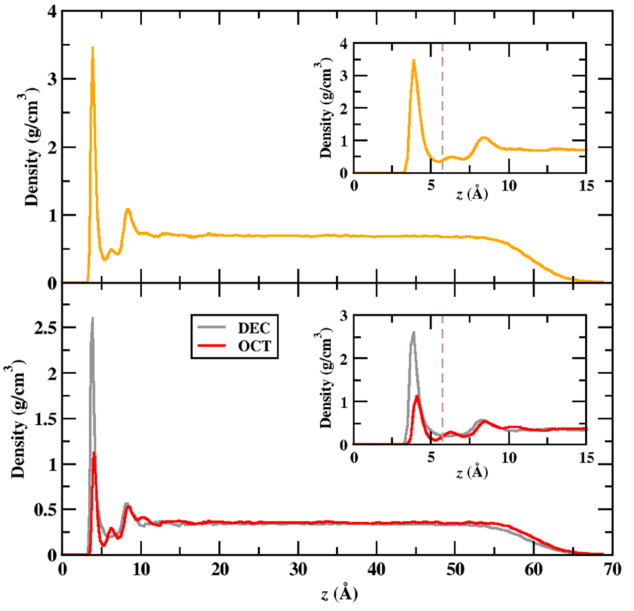

Figure 7. Centre-of-mass density profile for an equimolar mixture of DEC and OCT. The total density profile is shown at top (orange). In the bottom panel, the density profile for each molecule is shown. DEC is shown in grey and OCT is shown in red. Insets show the profile within 20 Å of the interface. The brown dashed line is at 5.75 Å, the cutoff used for orientational and surface adsorption analyses.

neat OCT (Figure 7). When the COM profiles for the two types of molecules are separated, it is clear that, as in the case of DEC–HEPT, DEC is preferentially adsorbed at the

interface. The united-atom bead density profile for this system is available in supporting information (Figure S1). Similar trends to those already observed are present in both the OCT–HEPT binary mixture and the solution of all three isomers (Figs. S2–S4).

3.2. Surface adsorption

The appearance of the mixture density profiles reflects the adsorption behaviour at the substrate–liquid interface. Adsorption at the substrate interface is characterised by the surface excess for component *i*, Γ_i, calculated from the fluid phase density according to Equation 1

$$\Gamma_i = \int_{z_0}^{z_1} \rho_i(z) - \rho_i^{\mathrm{b}} \, \mathrm{d}z \tag{1}$$

where z_0 is where the adsorbed density first equals the bulk density, z_1 is the edge of the liquid region before the vapour interface, and ρ_i^{b} is the average density of component *i* in the bulk liquid region [76]. For each system, z_0 was set to 3.5 Å. The edge of the liquid region was chosen at $z_1 = 50$ Å, which is below the vapour–liquid interface for all systems examined here. The bulk liquid density was calculated from $z = 25$ Å to $z = 50$ Å. A positive value of Γ_i means that the density of component *i* in the interfacial region is greater than the density of component *i* in the bulk liquid region, and, thus, there is an excess of *i* at the surface. The values of Γ_i are provided in Table 1.

All fluids show a total surface excess near 0.65 molecules/nm^2. Within the mixtures, there is a strong the preference for decane at the substrate interface, as is observed in the density profiles. The surface excess of DEC is nearly four or more times greater than the surface excess of either OCT or HEPT within the mixtures, despite all three having similar Γ values for the neat liquids.

3.3. Preferential adsorption

Additional analyses of these solutions focus on the behaviour of the liquid phase in the near vicinity of the solid substrate. We used the COM density profile for the ternary mixture in order to define which molecules are in different layers adjacent to the interface (Figure S4). In this profile, the first layer extends to 5.75 Å. In examining the neat COM density profiles, it is clear that this cutoff is a compromise across the three isomers (Figure 3). It will be used for all of the analyses of properties of the first molecular layers within the fluids simulated here to provide a standard basis for comparison.

In mixtures of normal alkanes, preferential adsorption of longer chain alkanes is observed both experimentally and computationally [34,38,86,88–90]. As the difference in chain length between the alkanes present increases, the enhanced adsorption of the longer chain molecule increases. Here, the molecules present are constitutional isomers leading to very different footprints at the interface. Table 2 provides the average number density of molecules absorbed at the interface for each simulation and the mole fraction enhancements/depletions, the ratio of the mole fraction in the layer to the bulk mole fraction, at both interfaces. Figures 1 and 2 show representative snapshots of the first layer of each fluid phase. The molecules shown are approximately equal to the average surface densities in Table 2.

In the mixtures, when decane is present, there is a clear preference for the adsorption of decane at the interface. Across the mixtures, the average total density of adsorbed species is constant within the uncertainty. Yet, when present, decane is observed at mole fractions well over 0.5, with mole fraction enhancements 1.32 and higher (Table 2). Consistent with earlier studies of linear alkanes, maximising interfacial interactions between substrate and liquid molecules, and, thus, adsorption enthalpy, dominates adsorption behaviour. DEC has the longest linear axis of the molecules represented here and no branch points, allowing for the strongest adsorption energies and tightest surface packing.

The only mixture for which preferential adsorption is not observed is the 1:1 mixture of OCT and HEPT. Here, there is a slight preference for HEPT to adsorb at the interface, but the preference is not as strong as for DEC. Note that for this mixture, the total density of molecules in the first layer is midway between the surface coverage for the two neat liquids.

Table 1. Surface excess, Γ_i, of component *i* at the solid interface. Subscripts denote the uncertainty in the last digit.

	Γ_i (molec/nm^2)			
Fluid	DEC	OCT	HEPT	Total
neat DEC	0.64_1			0.64_1
neat OCT		0.65_1		0.65_1
neat HEPT			0.65_1	0.65_1
DEC–OCT	0.61_2	0.04_2		0.65_1
DEC–HEPT	0.53_5		0.11_5	0.64_1
OCT–HEPT		0.29_3	0.36_3	0.65_1
DEC–OCT–HEPT	0.47_2	0.06_5	0.12_5	0.65_1

3.4. Molecular orientation

To more fully examine the behaviour of the liquid adjacent to the solid substrate, we next examined the molecular orientation of the fluid at the substrate interface. To identify the most likely molecular orientations at the interface, we looked first at the neat liquids in detail and

Table 2. Surface coverage density within the first layer adsorbed at the solid interface and mole fraction enhancements/depletions at the solid and vapour interfaces.[a] Subscripts denote the uncertainty in the last digit.

	Mole fraction enhancement/depletion						Average number density by			
	solid–liquid interface			vapour–liquid interface			molecule type (molecule/nm^2)			
Fluid	DEC	OCT	HEPT	DEC	OCT	HEPT	DEC	OCT	HEPT	TOTAL
neat DEC							1.26_1			1.26_1
neat OCT								1.23_1		1.23_1
neat HEPT									1.32_1	1.32_1
DEC–OCT	1.41_2	0.59_2		0.88_1	1.12_1		0.87_1	0.37_1		1.24_2
DEC–HEPT	1.32_5		0.68_5	0.95_1		1.05_1	0.84_3		0.43_3	1.27_6
OCT–HEPT		0.96_7	1.04_8		1.06_4	0.94_4		0.61_4	0.66_5	1.27_9
DEC–OCT–HEPT	1.53_6	0.71_3	0.76_5	0.88_1	1.12_1	1.00_1	0.65_2	0.30_1	0.32_2	1.27_6

[a]The solid–liquid interface includes molecules with $z_{COM} < 5.75$ Å. The vapour–liquid interface includes all molecules within the Gibbs dividing surface as defined in Table S2.

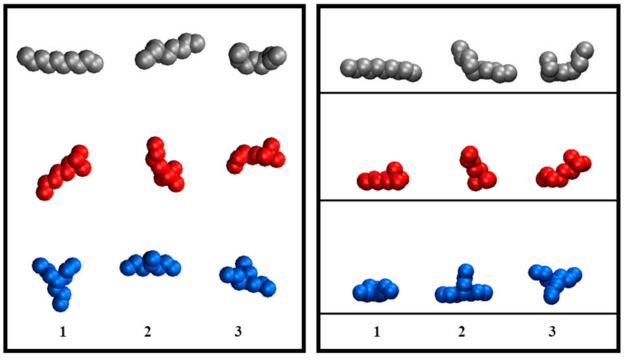

Figure 8. Top (left) and side (right) views of orientations 1, 2, and 3 for DEC (grey; top), OCT (red; middle), and HEPT (blue; bottom). Descriptions of each orientation are provided in the text.

compared the relative orientations of adsorbed molecules within the mixtures to these distributions.

We defined three main orientations for each type of molecule in this interfacial region. The nine orientations discussed below are shown in Figure 8. The first orientation for each molecule was the orientation that included the largest proportion of the molecule, in terms of united-atom beads, adjacent to the solid substrate. Here, these molecules are identified by the number of CH_3 beads within the first layer region. For DEC, this means that both ends of the molecule are within 5.75 Å of the interface. For OCT, the CH_3 bead at the end of the hexyl tail as well as at least two of the three CH_3 beads in the head group are all within 5.75 Å of the interface. For HEPT, this includes all three CH_3 groups lying within 5.75 Å of the substrate.

In the remaining orientations for each, the molecule extends beyond the first layer. For DEC, only one of the two CH_3 groups is found within the first layer cutoff for the second orientation. A third possibility features the middle portion of the molecule within 5.75 Å of the surface but the both CH_3 groups outside this cutoff. The two additional orientations for OCT account for the head group being in either the first or second layer with the hexyl tail primarily in the opposite layer as defined by the CH_3 bead location. In orientation 2, the *t*-butyl head group is orientated such that all three CH_3 groups are at the interface and the tail CH_3 points away. In orientation 3, the opposite is true, with the *t*-butyl group pointing away from the interface. Similarly, for HEPT, the two additional orientations take into account whether two propyl 'arms' (orientation 2) or one propyl 'arm' (orientation 3) are in the first layer region.

The relative frequencies of these orientations in each fluid phase are provided in Table 3. As noted previously, these data include only molecules with the COM within 5.75 Å. Fewer than 0.1% of molecules fitting this criterion in any of the seven liquid phases are not represented by one of the nine orientations evaluated.

For DEC and OCT, the most common orientation features the molecular axis parallel to the substrate (orientation 1). This maximises the energy of interaction between the adsorbed molecule and the substrate (Table 4). These alignments also allow for higher packing efficiency, as noted by Wang and Fichthorn [30]. The other 16% and 28% of molecules for OCT and DEC, respectively, adopt orientations where at least one end of the molecule is outside of the first layer cutoff. These 'pillar' molecules were also observed by Wang and Fichthorn in their simulations of OCT.

For HEPT, the first and second orientations are observed at a nearly equal likelihood. While the average energy of adsorption for the first orientation is the most favourable, this orientation has a very large footprint at the interface (Table 4, Figure 8). When HEPT molecules are absorbed such that they are nearly planar and parallel to the interface, as in orientation 1, less space is available for other molecules to interact with the surface. In orientation 2, the majority of the molecule is still directly adjacent to the substrate but the more surface area is available for other molecules to approach the interface. The overall adsorption energy may be lowered by allowing more molecules to get closer to the substrate, even

Table 3. Fraction of molecules adopting specific orientations relative to the substrate at the solid–liquid interface.[a] Subscripts denote the uncertainty in the last digit.

	Decane			2,2-Dimethyloctane			4-Propylheptane		
Fluid	1	2	3	1	2	3	1	2	3
neat DEC	0.723_1	0.267_1	0.011_1						
neat OCT				0.839_1	0.086_1	0.073_1			
neat HEPT							0.506_1	0.480_1	0.014_1
DEC–OCT	0.738_3	0.253_1	0.010_1	0.821_5	0.095_1	0.082_1			
DEC–HEPT	0.739_4	0.251_1	0.010_1				0.486_5	0.499_4	0.015_1
OCT–HEPT				0.838_7	0.088_1	0.071_1	0.510_5	0.476_5	0.013_1
DEC–OCT–HEPT	0.736_4	0.254_1	0.009_1	0.827_4	0.093_1	0.079_1	0.495_6	0.490_4	0.015_1

[a]Representations of chosen orientations are shown in Figure 8. The solid–liquid interface includes molecules with $z_{COM} < 5.75$ Å.

Table 4. Adsorption energy for different molecular orientations within the first adsorbed layer for each isomer.[a] Subscripts denote the uncertainty in the last digit.

	Average interaction energy (kJ/mol)		
Orientation	DEC	OCT	HEPT
1	-46_6	-39_5	-44_5
2	-33_6	-27_6	-32_5
3	-27_5	-27_4	-22_4

[a]Representations of chosen orientations are shown in Figure 8. The first adsorbed layer includes molecules with $z_{COM} < 5.75$ Å.

though this does not maximise the adsorption interaction for any given molecule of HEPT. In Table 2, the fluids with the highest surface density of molecules always have HEPT present. This observation is consistent with the adoption of a smaller-footprint orientation by a large portion of the interfacial molecules.

The presence of more than one type of decane isomer in the fluid phase has little to no impact on the distribution of molecular orientations observed among the adsorbed molecules (Table 3). The preferred orientations of the molecules at the interface are strongly influenced by the energy of attraction between the molecules and the substrate (Table 4). In each case, the lowest energy conformation is also the most common orientation and the fraction of molecules in a given orientation generally decreases with increasing interaction energy. Adsorption energy, though, is not sufficient to explain all of the trends observed with respect to molecular orientation.

Examining the in-plane two-dimensional ordering for both neat liquids and mixtures, we observe fewer regions of 2D alignment as compared to films of longer *n*-alkanes [34,38,60]. In their simulations of *n*-hexadecane/*n*-hexane mixtures, Math *et al.* [38] observe *n*-hexadecane adopting ordered domain regions at a smooth interface with *n*-hexane interspersed between adjacent domains. Our previous work [34] showed that for *n*-octane/*n*-nonane and *n*-octane/*n*-dodecane mixtures, few molecule-specific domains were observed, but there was a general preference for all molecules to align with adjacent molecules regardless of species.

In the current simulations, the presence of the side chains impacts the two-dimensional alignment of adjacent molecules. We looked for domains at the interface where two or more molecules were aligned such that their centres of mass were within 7 Å and the cosine of the angle between their long molecular axis vectors was greater than 0.9, which corresponds to an angle less than 25.8°. Table 5 presents the results of this analysis. First, we note that the presence of DEC or OCT greatly increases the percentage of molecules with at least one aligned neighbour. For HEPT, 93% of molecules are not aligned with other species at the interface. Examination of the snapshot of the HEPT surface in Figure 1 supports this finding. Additionally, the presence of HEPT at the interface reduces the overall alignment in general when comparing the three binary solutions.

Among the domains present, in most cases, alignment exists between only two molecules given the criteria used here. In all cases, more than 70% of the aligned domains present consist of pairs of molecules. Consistent with previous studies of linear alkanes, for DEC we see the greatest degree and extent of alignment with nearly half of all molecules aligned with a neighbour in the neat liquid and 30% of the aligned domains consisting of three or more molecules. The type of branching present in the isomers greatly impacts the molecular alignment. In the DEC–OCT solution, the extent and degree of alignment is very similar to the neat DEC liquid and slightly greater than the neat OCT liquid. When HEPT is introduced, though, the degree of domain formation drops sharply with fewer than 30% of molecules aligned in the DEC–HEPT solution. In contrast to the neat HEPT liquid, though, this degree of ordering is substantial. More than two-thirds of these aligned pairs in the DEC–HEPT solution consist of only one type of molecule, primarily DEC whereas for the DEC–OCT solution, more than 40% are aligned DEC–OCT pairs.

Two–dimensional COM radial distribution functions for the solid–liquid and liquid–vapour interfaces, and a region in the bulk fluid, are available in supporting information for comparison (Figs. S5–S7). Consistent with

Table 5. Distribution of domain sizes for groups of molecules with parallel alignment of the long molecular axes of adjacent molecules at the solid–liquid interface.[a] Subscripts denote the uncertainty in the last digit.

Fluid	Fraction of molecules with one or more aligned neighbours	Distribution of domain sizes				
		2	3	4	5	> 5
neat DEC	0.459_4	0.701_1	0.207_5	0.065_3	0.019_1	0.008_1
neat OCT	0.391_9	0.768_8	0.182_7	0.040_2	0.008_1	0.002_1
neat HEPT	0.070_3	0.942_2	0.054_2	0.004_3	0.001_1	
DEC–OCT	0.436_7	0.719_{10}	0.204_5	0.055_4	0.015_2	0.007_1
DEC–HEPT	0.289_{14}	0.792_{18}	0.169_{11}	0.030_5	0.007_2	0.002_1
OCT–HEPT	0.188_9	0.862_7	0.122_7	0.014_2	0.002_1	0.001_1
DEC–OCT–HEPT	0.319_8	0.776_8	0.169_4	0.042_3	0.011_2	0.002_1

[a]The solid–liquid interface includes molecules with $z_{COM} < 5.75$ Å.

the domain analysis, there is little preference for specific neighbouring molecule types, particularly in the bulk and liquid–vapour interfacial regions. When present, HEPT exhibits some preference for interaction with other HEPT molecules, but the domain analysis shows that this does not extend to molecular axis alignment between the molecules.

3.5. Vapour–liquid interface

Each system modelled here also features a vapour–liquid interface above $z = 55$ Å following a bulk liquid region. An examination of the COM density profile for each system shows that this interface is significantly more diffuse than the solid–liquid interface and no density oscillations are observed (see Figs. 3,5,7, S2 and S4). To examine the behaviour of the system at the vapour–liquid interface, a hyperbolic tangent fit to the total COM density profile was used to determine the position of the Gibbs dividing surface (GDS), z_{GDS}, and the width of the interface, δ_{GDS},

$$\rho(z) = \frac{\rho_{liq} + \rho_{vap}}{2}\left[1 - \tanh\left(\frac{z - z_{GDS}}{\delta_{GDS}}\right)\right] \quad (2)$$

where ρ_{liq} and ρ_{vap} are the densities of the bulk liquid and vapour phases, respectively. The interface is defined using the '10-90' range of the liquid density [91,92]. The position and width of the GDS for each system, as well as the bulk liquid and vapour densities and vapour pressure, are provided in the supporting information (Table S2).

The mole fraction enhancement for each mixture at the vapour–liquid interface is provided in Table 2. When present, OCT is preferentially found within the 10-90 interfacial region. The surface tension of branched alkanes is generally less than that of linear alkanes as a result of weaker intermolecular forces for the branched isomers [93–96]. A strong enhancement of OCT, and HEPT when it is the only branched alkane present, at the interface results. In contrast to the liquid–solid interface, no orientational preference is observed here. A comparison of the distribution of molecules as a function of the angle between the long axis of the molecule and the surface normal at the liquid–solid interface, bulk, and vapour–liquid interface for the ternary system is available in supporting information (Figure S8) for reference.

4. Conclusions

Using Monte Carlo simulations, we showed that molecular geometry has a strong impact on surface adsorption from liquids at a solid metal surface, particularly as branch length increases. At the interface, favourable interactions between the adsorbed molecule and the substrate drive both preferential adsorption and preferences in molecule orientation upon adsorption. With the introduction of branched molecules, the interplay between entropic and enthalpic driving forces for adsorption shifts from enthalpic for linear alkanes towards entropic factors as the degree of branching increases. In equimolar solutions, the enthalpic gain from parallel adsorption, both with respect to the substrate and to neighbouring molecules, of *n*-decane at the interface dominates over the entropic gain of more molecules adsorbed at the interface as observed in 4-propylheptane. Strong preferential adsorption of *n*-decane was observed in all mixtures studied here. Without decane present, though, no preferential adsorption was observed for the remaining isomers.

Acknowledgements

The authors thank Katie Maerzke for helpful feedback during the preparation of this manuscript.

Disclosure statement

No potential conflict of interest was reported by the author(s).

Funding

This work was supported by the donors of ACS Petroleum Research Fund Undergraduate New Investigator Grant 50559-UNI6 and the Thomas F. and Kate Miller Jeffress Memorial Trust under Grant J-989. Computational resources were provided in part by the MERCURY consortium (https://mercury

consortium.org/) under NSF grants CHE-1229354, CHE-1662030, and CHE-2018427.

ORCID

Kelly E. Anderson http://orcid.org/0000-0002-2809-6716

References

[1] F. Zaera, Chem. Rev. **112**, 2920–2986 (2012). doi:10.1021/cr2002068
[2] D.M. Cyr, B. Venkataraman and G.W. Flynn, Chem. Mater. **8**, 1600–1615 (1996). doi:10.1021/cm960113a
[3] E. Bonaccurso, M. Kappl and H.J. Butt, Curr. Opin. Colloid Interface Sci. **13**, 107–119 (2008). doi:10.1016/j.cocis.2007.11.010
[4] H. Kern, W.V. Rybinski and G.H. Findenegg, J. Coll. Interface Sci. **59**, 301–307 (1977). doi:10.1016/0021-9797(77)90012-1
[5] H.K. Christenson, D.W.R. Gruen, R.G. Horn and J.N. Israelachvili, J. Chem. Phys. **87**, 1834–1841 (1987). doi:10.1063/1.453196
[6] J.N. Israelachvili, Acc. Chem. Res. **20**, 415–421 (1987). doi:10.1021/ar00143a005
[7] S. Balasubramanian, M.L. Klein and J.I. Siepmann, J. Chem. Phys. **100**, 11960–11963 (1996). doi:10.1021/jp9608887
[8] W.J. Huisman, J.F. Peters, M.J. Zwanenburg, S.A. de Vries, D. Abernathy and J.F. van der Veen, Nature **390**, 379–381 (1997). doi:10.1038/37069
[9] C.J. Yu, A.G. Richter, A. Datta, M.K. Durbin and P. Dutta, Phys. Rev. Lett. **82**, 2326–2329 (1999). doi:10.1103/PhysRevLett.82.2326
[10] D. Woywod and M. Schoen, J. Phys.: Condens. Matter **16**, 4761–4783 (2004).
[11] O. Pizio, S. Sokołowski and Z. Sokołowska, J. Chem. Phys. **134**, 214702 (2011). doi:10.1063/1.3597773
[12] S. Materniak and A. Patrykiejew, J. Chem. Phys. **139**, 014705 (2013). doi:10.1063/1.4812370
[13] M. Heier, S. Stephan, F. Diewald, R. Müller, K. Langenbach and H. Hasse, Langmuir **37**, 7405–7419 (2021). doi:10.1021/acs.langmuir.1c00780
[14] C.J. Segura, J. Zhang and W.G. Chapman, Molec. Phys. **99**, 1–12 (2001). doi:10.1080/00268970109483483
[15] J.R. Silbermann, D. Woywod and M. Schoen, Phys. Rev. E **69**, 031606 (2004). doi:10.1103/PhysRevE.69.031606
[16] D. Woywod, S. Schemmel, G. Rother, G.H. Findenegg and M. Schoen, J. Chem. Phys. **122**, 124510 (2005). doi:10.1063/1.1867372
[17] M. Heier, F. Diewald, R. Müller, K. Langenbach and H. Hasse, J. Chem. Eng. Data **66**, 3722–3734 (2021). doi:10.1021/acs.jced.1c00350
[18] F. Schmid and N.B. Wilding, Phys. Rev. E **63**, 031201 (2001). doi:10.1103/PhysRevE.63.031201
[19] A. Patrykiejew, Eur. Phys. J. B **91**, 210 (2018). doi:10.1140/epjb/e2018-90304-5
[20] M. Areshi, D. Tseluiko, U. Thiele, B.D. Goddard and A.J. Archer, Phys. Rev. E **109**, 024801 (2024). doi:10.1103/PhysRevE.109.024801
[21] A.K. Doerr, M. Tolan, J.P. Schlomka and W. Press, Europhys. Lett. **52**, 330–336 (2000). doi:10.1209/epl/i2000-00443-7
[22] M. Buzzacchi, I. Pagonabarraga and N.B. Wilding, J. Chem. Phys. **121**, 11362–11373 (2004). doi:10.1063/1.1818020
[23] M. Buzzacchi, N.B. Wilding and P. Sollich, Phys. Rev. Lett. **97**, 136104 (2006). doi:10.1103/PhysRevLett.97.136104
[24] X. Chen, L. Sun, H. Liu, Y. Hu and J. Jiang, J. Chem. Phys. **131**, 044710 (2009). doi:10.1063/1.3191783
[25] L. Wu, A. Malijevsky, C. Avendano, E.A. Mükker and G. Jackson, J. Chem. Phys. **148**, 164701 (2018). doi:10.1063/1.5020002
[26] E.L. Granados-Bazán, S.E. Quinones-Cisneros and U.K. Deiters, Langmuir **37**, 10945 (2021). doi:10.1021/acs.langmuir.1c01354
[27] T.K. Xia, J. Ouyang, M.W. Ribarsky and U. Landman, Phys. Rev. Lett. **69**, 1967–1970 (1992). doi:10.1103/PhysRevLett.69.1967
[28] R. Hentschke and R.G. Winkler, J. Chem. Phys. **9**, 5528–5534 (1993). doi:10.1063/1.465971
[29] S. Balasubramanian, M.L. Klein and J.I. Siepmann, J. Chem. Phys. **103**, 3184–3194 (1995). doi:10.1063/1.470251
[30] J.C. Wang and K.A. Fichthorn, J. Chem. Phys. **108**, 1653–1663 (1998). doi:10.1063/1.475536
[31] J.C. Wang and K.A. Fichthorn, J. Chem. Phys. **116**, 410–417 (2002). doi:10.1063/1.1419258
[32] J. Cousty and L. Pham Van, Phys. Chem. Chem. Phys. **5**, 599–603 (2003). doi:10.1039/b206529k
[33] C. Wei, Phys. Rev. B **80**, 085409 (2009). doi:10.1103/PhysRevB.80.085409
[34] S. Wenzel, H. Nemec, K.E. Anderson and J.I. Siepmann, Langmuir **30**, 3086–3094 (2014). doi:10.1021/la4048598
[35] H.K. Chilukoti, G. Kikkugawa and T. Ohara, RSC Adv. **6**, 99704 (2016). doi:10.1039/C6RA22398B
[36] J. Liu, L. Wang, S. Xi, D. Asthagiri and W.G. Chapman, Langmuir **33**, 11189–11202 (2017). doi:10.1021/acs.langmuir.7b02055
[37] D.C.J. de Andrade and B. Nojabaei, Nanomaterials **11**, 2431 (2021). doi:10.3390/nano11092431
[38] S. Math, J. Gao and U. Landman, J. Phys. Chem. C **126**, 4209–4219 (2022). doi:10.1021/acs.jpcc.1c10471
[39] A.N. Vasilyuk and R.M. Lynden-Bell, Molec. Phys. **99**, 1407–1411 (2001). doi:10.1080/00268970110061810
[40] J. Bowers, A. Zarbakhsh, H.K. Christenson, I.A. McLure and R. Cubitt, J. Chem. Phys. **119**, 11917–11925 (2003). doi:10.1063/1.1624826
[41] G.M. Leuty and M. Tsige, J. Phys. Chem. B **115**, 12694–12708 (2011). doi:10.1021/jp2057139
[42] J. Di, Z. Yang and Y. Duan, AIP Adv. **11**, 045104 (2021). doi:10.1063/5.0043039
[43] M. Lundgren, N.L. Allan and T. Cosgrove, Langmuir **18**, 10462–10466 (2002). doi:10.1021/la026191w
[44] D. Surblys, Y. Yamaguchi, K. Kuroda, M. Kagawa, T. Nakajima and H. Fujimura, J. Chem. Phys. **140**, 034505 (2014). doi:10.1063/1.4861039
[45] S. Nakaoka, Y. Yamaguchi, T. Omori, M. Kagawa, T. Nakajima and H. Fujimura, Phys. Rev. E **92**, 022402 (2015). doi:10.1103/PhysRevE.92.022402
[46] M.F. Harrach, B. Drossel, W. Winschel, T. Gutmann and G. Buntkowsky, J. Phys. Chem. C **119**, 28961–28969 (2015). doi:10.1021/acs.jpcc.5b09537
[47] N. Safaei and A. Maghari, J. Stat. Mech. **2015**, P06033 (2015). doi:10.1088/1742-5468/2015/06/P06033

[48] B. Kumari, M. Brodrecht, H. Breitzke, M. Werner, B. Grünberg, H.H. Limbach, S. Forg, E.P. Sanjon, B. Drossel, T. Gutmann and G. Buntkowsky, J. Phys. Chem. C **122**, 19540–19550 (2018). doi:10.1021/acs.jpcc.8b04745
[49] J. Xu, L. Jia, C. Dang, X. Liu and Y. Ding, AIP Adv. **12**, 105313 (2022). doi:10.1063/5.0120656
[50] M. Takayanagi, N. Fujiwara, R. Seki, M. Sato and Y. Okuno, ECS J. Solid State Sci. Technol. **12**, 083003 (2023). doi:10.1149/2162-8777/acec0e
[51] J. Rodriguez, M.D. Elola and D. Laria, J. Phys. Chem. B **113**, 12744–22749 (2009). doi:10.1021/jp905920m
[52] J. Rodriguez, M.D. Elola and D. Laria, J. Phys. Chem. B **114**, 7900–7908 (2010). doi:10.1021/jp101836b
[53] S.M. Melnikov, A. Höltzel, A. Seidel-Morgenstern and U. Tallarek, Anal. Chem. **83**, 2569–2575 (2011). doi:10.1021/ac102847m
[54] S. Melnikov, A. Höltzel, A. Seidel-Morgenstern and U. Tallarek, Angew. Chem. Intl. Ed. **51**, 6251–6254 (2012). doi:10.1002/anie.v51.25
[55] N. Kumar, S. Singla, M.C. Wilson, S. Kaur, S. Bekele, M. Tsige and A. Dhinojwala, J. Phys. Chem. C **123**, 29729–29738 (2019). doi:10.1021/acs.jpcc.9b09019
[56] M.M. Koleini, M.H. Badizad, H. Mahani, A.M. Dastjerdi, S. Ayatollahi and M.H. Ghazanfari, Sci. Rep. **11**, 11967 (2021). doi:10.1038/s41598-021-91402-0
[57] S.J. O'Shea, M.E. Welland and T. Rayment, Appl. Phys. Lett. **60**, 2356–2358 (1992). doi:10.1063/1.107024
[58] J.N. Israelachvili, *Intermolecular and Surface Forces*, 3rd ed. (Elsevier, Waltham, MA, 2011).
[59] T. Ondarchu and J.P. Aime, *Nanoscale Liquid Interfaces* (Pan Stanford Publishing, Singapore, 2013).
[60] J.J. Potoff and J.I. Siepmann, Langmuir **18**, 6088–6095 (2002). doi:10.1021/la011581o
[61] N.N. Gosvami, S.K. Sinha and S.J. O'Shea, Phys. Rev. Lett. **100**, 076101/1–4 (2008). doi:10.1103/PhysRevLett.100.076101
[62] D. Fuhrmann, A.P. Graham, L. Criswell, H. Mo, B. Matthies, K.W. Herwig and H. Taub, Surf. Sci. **482-485**, 77–82 (2001). doi:10.1016/S0039-6028(01)00925-6
[63] Monte Carlo for Complex Chemical Systems-MN http://siepmann.chem.umn.edu/software.
[64] J.I. Siepmann and D. Frenkel, Molec. Phys. **75**, 59–70 (1992). doi:10.1080/00268979200100061
[65] J.J. de Pablo, M. Laso, J.I. Siepmann and U.W. Suter, Molec. Phys. **80**, 55–63 (1993). doi:10.1080/00268979300102061
[66] M.G. Martin and J.I. Siepmann, J. Phys. Chem. B **103**, 4508–4517 (1999). doi:10.1021/jp984742e
[67] J.I. Siepmann and I.R. McDonald, Molec. Phys. **75**, 255–259 (1992). doi:10.1080/00268979200100201
[68] J.M. Stubbs and J.I. Siepmann, J. Phys. Chem. B **106**, 3968–3978 (2002). doi:10.1021/jp013759l
[69] M.G. Martin and J.I. Siepmann, J. Phys. Chem. B **102**, 2569–2577 (1998). doi:10.1021/jp972543+
[70] N.D. Zhuravlev and J.I. Siepmann, Fluid Phase Equil. **134**, 55–61 (1997). doi:10.1016/S0378-3812(97)00029-0
[71] MolMod Database http://molmod.boltzmann-zuse.de/.
[72] S. Stephan, M.T. Horsch, J. Vrabec and H. Hasse, Mol. Simul. **45**, 806–814 (2019). doi:10.1080/08927022.2019.1601191
[73] S. Schmitt, F. Fleckenstein, H. Hasse and S. Stephan, J. Phys. Chem. B **127**, 1789–1802 (2023). doi:10.1021/acs.jpcb.2c07997
[74] K.M. Benjamin, A. Asiaee, C. Veer, C. Losinski, S. Gunderson and T. Larson, J. Phys. Chem. C **120**, 21336–21343 (2016). doi:10.1021/acs.jpcc.6b03108
[75] M. Dinpajooh, P. Bai, D.A. Allan and J.I. Siepmann, J. Chem. Phys. **143**, 114113/1–13 (2015).
[76] M. Heier, F. Diewald, M.T. Horsch, K. Langenbach, R. Müller and H. Hasse, J. Chem. Eng. Data **64**, 386–394 (2019). doi:10.1021/acs.jced.8b00927
[77] A. Hubao, Z. Yang, R. Hu, Y.F. Chen and L. Yang, J. Phys. Chem. C **124**, 23260–23269 (2020). doi:10.1021/acs.jpcc.0c07919
[78] E. Bertrand, T.D. Blake and J.D. Coninck, J. Phys.: Condens. Matter **21**, 464124 (2009).
[79] S. Chatterjee, A. Singh and M. Chakraborty, Langmuir **2023**, 4789–4798 (2023). doi:10.1021/acs.langmuir.3c00167
[80] R. Wang, S. Bi, V. Presser and G. Feng, Fluid Phase Equil. **463**, 106–113 (2018). doi:10.1016/j.fluid.2018.01.024
[81] T.D. Blake and J.D. Coninck, Adv. Colloid Interface **96**, 21–36 (2002). doi:10.1016/S0001-8686(01)00073-2
[82] J. Hautman and M.L. Klein, J. Chem. Phys. **91**, 4994–5001 (1989). doi:10.1063/1.457621
[83] Y. Wang, K. Hill and J.G. Harris, Langmuir **9**, 1983–1985 (1993). doi:10.1021/la00032a014
[84] J.J. Potoff and J.I. Siepmann, Phys. Rev. Lett. **85**, 3460 (2000). doi:10.1103/PhysRevLett.85.3460
[85] C.J. Mundy, S. Balasubramanian, K. Bagchi, J.I. Siepmann and M.L. Klein, Faraday Discuss. **104**, 17–36 (1996). doi:10.1039/fd9960400017
[86] P. Smith, R.M. Lynden-Bell and W. Smith, Molec. Phys. **98**, 255–260 (2000). doi:10.1080/00268970009483289
[87] M. Krishnan, S. Balasubramanian and S. Clarke, Proc. Indian Acad. Sci. (Chem. Sci.) **115**, 663–677 (2003). doi:10.1007/BF02708256
[88] M.A. Castro, S.M. Clarke, A. Inaba, T. Arnold and R.K. Thomas, J. Phys. Chem. B **102**, 10528–10534 (1998). doi:10.1021/jp982965z
[89] M.A. Castro, S.M. Clarke, A. Inaba, T. Arnold and R.K. Thomas, Phys. Chem. Chem. Phys. **1**, 5017–5023 (1999). doi:10.1039/a906184c
[90] M.A. Castro, S.M. Clarke, A. Inaba, R.K. Thomas and T. Arnold, J. Phys. Chem. B **105**, 8577–8582 (2001). doi:10.1021/jp010873v
[91] A. Zangwill, *Physics at Surfaces* (Cambridge University Press, Cambridge, UK, 1988).
[92] A.W. Adamson and A.P. Gast, *Physical Chemistry of Surfaces*, 6th ed. (Wiley-Interscience, New York, 1997).
[93] J.A. Riddick, W.B. Bunger and T. Sakano, *Organic Solvents: Physical Properties and Methods of Purification*, 4th ed. (John Wiley & Sons, New York, 1986).
[94] T. Klein, J. Cui, A. Kalantar, J. Chen, M.H. Rausch, T.M. Koller and A.P. Fröba, J. Chem. Eng. Data **63**, 2833–2839 (2018). doi:10.1021/acs.jced.8b00163
[95] T. Klein, S. Yan, J. Chen, J.W. Magee, K. Kroenlein, M.H. Rausch, T.M. Koller and A.P. Fröba, J. Chem. Eng. Data **64**, 4116–4131 (2019). doi:10.1021/acs.jced.9b00525
[96] T. Klein, F.D. Lenahan, M. Kerscher, M.H. Rausch, I.G. Economou, T.M. Koller and A.P. Fröba, J. Phys. Chem. B **124**, 4146–4163 (2020). doi:10.1021/acs.jpcb.0c01740